Journal of Magnetic Resonance 263 (2016) 136–146

Contents lists available at ScienceDirect

Journal of Magnetic Resonance

journal homepage: www.elsevier.com/locate/jmr

Spatially resolved spectroscopy using tapered stripline NMR

Koen C.H. Tijssen [a], Jacob Bart [a], Roald M. Tiggelaar [b], J.W.G. (Hans) Janssen [a], Arno P.M. Kentgens [a], P. Jan M. van Bentum [a,*]

[a] Institute for Molecules and Materials, Radboud University, Nijmegen, The Netherlands
[b] Mesa+ Institute for Nanotechnology, University of Twente, Enschede, The Netherlands

ARTICLE INFO

Article history:
Received 28 October 2015
Revised 15 December 2015
Available online 8 January 2016

Keywords:
NMR
Tapered stripline
B_1 imaging
RF gradient
Reaction monitoring
Microfluidics
RF coil design

ABSTRACT

Magnetic field B_0 gradients are essential in modern Nuclear Magnetic Resonance spectroscopy and imaging. Although RF/B_1 gradients can be used to fulfill a similar role, this is not used in common practice because of practical limitations in the design of B_1 gradient coils. Here we present a new method to create B_1 gradients using stripline RF coils. The conductor-width of a stripline NMR chip and the strength of its radiofrequency field are correlated, so a stripline chip can be tapered to produce any arbitrary shaped B_1 field gradient. Here we show the characterization of this tapered stripline configuration and demonstrate three applications: magnetic resonance imaging on samples with nL–μL volumes, reaction monitoring of fast chemical reactions (10^{-2}–10^{1} s) and the compensation of B_0 field gradients to obtain high-resolution spectra in inhomogeneous magnetic fields.

1. Introduction

In general microcoils for the detection of nL–μL samples are often compromised in spectral resolution. This is due to manufacturing imperfections and very local distortions, i.e. magnetic susceptibility differences of materials [1]. In recent years, we have introduced an alternative stripline-based NMR probe as a route to high-resolution NMR on nanoliter samples [2,3].

An interesting property of striplines, which makes them especially attractive for magnetic resonance imaging (MRI) purposes, is that the local RF field strength above the stripline is directly related to the width of the stripline. This means that, by introducing a tapered modification of the stripline, well-defined arbitrary B_1 gradients are attainable, which can be used to impose a spatial coding of spins along this taper. Using a simple 2D nutation experiment, a 1D-image can be recorded with uncompromised spectral (chemical shift) information. Although MRI is traditionally based on the use of B_0 gradients instead of B_1 gradients, the use of these RF gradients has been explored before [4,5], but its implementation was difficult because of limitations in RF gradient design.

One of the proposed applications for stripline NMR is the analysis of fast chemical reaction kinetics. Using uniform B_1-field stripline NMR, we already demonstrated [6] that chemical reactions can be monitored in a time range of seconds to tens of minutes. By adjusting the flow rates of the reactants, the delay between mixing and NMR detection can be varied, which translates into a time axis for the ongoing reaction. The main limitation in this system was the finite pathway from the microreactor to the NMR chip, which limited the minimum observable reaction time to about 4.5 s. Many chemical reactions, however, take place at sub-second time-scales, which are beyond the capability of this system.

In this manuscript, we will introduce the design and characterization of tapered striplines that aim at the generation of strong B_1 fields with arbitrary (including linear) gradients along a single axis. As a first application we use these gradients for imaging of small volume (nL–μL) samples. In a second application we use this alternative way of 1D-imaging for fast *in-situ* reaction screening. We demonstrate that the tapered stripline provides combined chemical structure information and spatial mapping, which allows for reaction profiling on a sub-second time-scale. As a third application we propose to use the perfect control over the shape of the tapered stripline's B_1 profile to perform NMR experiments in inhomogeneous magnetic fields without loss of spectral information.

2. Experimental section

2.1. Chemicals and materials

Unless stated otherwise, all samples were prepared in fused silica capillaries (Polymicro Technologies) with an inner diameter (ID) of 250 μm and an outer diameter (OD) of 360 μm. FC-40

* Corresponding author.
E-mail address: j.vanbentum@nmr.ru.nl (P.J.M. van Bentum).

http://dx.doi.org/10.1016/j.jmr.2015.12.021
1090-7807/

(Fluorinert), imidazole, deuterium oxide (D_2O), dimethylformamide (DMF) and phosphoryl chloride ($POCl_3$) were obtained from Sigma–Aldrich. Ethanol was obtained from Merck. 1-Propanol was obtained from Riedel-de Haën. All chemicals were used as received. For the reaction monitoring experiments 1 mL gas tight syringes (VWR 549-0536) were used and connected to the capillaries via a PEEK luer lock connector coupled to a one-piece finger-tight PEEK nut with a FEP sleeve between the nut and the capillary that matches either the 360 μm or 200 μm OD (IDEX Health & Science, P-659, F-120, F-242 and F-239 respectively). Connections between two or three capillaries were made using PEEK unions or T-connectors (IDEX Health & Science, P-779 and P-727 respectively). For pumping two syringe pumps (New Era, NE-1000) were used.

2.2. Tapered stripline chips

In this paper several different tapered stripline chips were used, numbered 1 to 3. Pictures (Fig. S6) and schematic cross sections (Fig. S5) of the tapered stripline chips and probes can be found in the Supplementary information. More detailed information about the fabrication of stripline chips can be found in work of Oosthoek-de Vries et al. [7].

Chip 1: For simple feasibility purposes, a 10 mm long tapered stripline (tapered from 3 to 1 mm) was fabricated using low-loss polytetrafluoroethylene (PTFE) based Printed Circuit Board (PCB, Rogers RT/duroid 5870). The PCB thickness was 0.254 mm, with a copper cladding at both sides of 17 μm. The stripline was structured by CNC milling with a 0.25 mm mill. Samples were positioned on top of the stripline in a second PCB from which the copper was removed at one side. For MRI testing purposes, four silicone rubber disks sample chambers were fabricated by drilling four holes with a diameter of 0.25 mm and a depth of 0.25 mm at a distance of 2 mm between each hole. The stripline was implemented as a short in a $\lambda/4$ resonator, resonant at 144 MHz.

Chip 2: High-resolution tapered stripline chips were fabricated on fused silica. The chip substrate was 35 mm long and 14 mm wide, the stripline constriction is 10 mm long and tapered from 5 to 1 mm in width. The structured copper stripline was defined on 500 μm thick fused silica wafers using photolithography, magnetron sputtering and electroplating [2]. To minimize susceptibility distortions, fluorinated ethylene propylene (FEP) was hot-pressed into copper-free areas on the chip. A channel for capillary alignment was fabricated by dicing (400 μm wide, 350 μm deep) into a second fused silica layer bonded to the copper. The stripline geometry was implemented as a short in a 3/4 lambda resonator, resonant at 600 MHz.

Chip 3: a 15 mm long stripline on fused silica, tapered from 5 to 1 mm, with the same substrate dimensions as chip 2. The chip was produced with the same techniques on the same fused silica wafers as chip 2. Only the second fused silica layer was omitted, instead two Teflon spacers, located at the ends of the chip, were used to space a copper ground plate from the structured layer in the center. The stripline was implemented as a short in a 3/4 lambda resonator, resonant at 400 MHz.

In all probes the tapered stripline chip is connected to a coaxial copper tube, which is part of the resonating system. The 1/4 or 3/4 lambda resonator has thus roughly the same length as the probe (Fig. S6) and the length of the taper is only a small fraction of the length of the full resonator, therefore the current can be assumed to remain constant along the z-axis of the taper.

2.3. NMR experiments and data treatment

The RF field strength profile and sensitivity profile of the tapered stripline were measured using ^{1}H NMR at 400 MHz on a 9.4 T solid-state NMR (Agilent-Varian) system with a tapered stripline probe containing chip 3. We characterized these profiles by moving a long sample capillary (ID: 250 μm, OD: 360 μm) in steps over the taper and performing a nutation experiment after every displacement. The top part of the capillary was filled with water. Copper sulfate was added to the water to reduce the T_1 (to 16.4 ms) and speed up the experiment. The other part of the capillary was filled with FC-40, a proton-free liquid which is a mixture of perfluorocarbons and is immiscible with water. The capillary was closed off with wax and UV-curable glue, and it was positioned inside the tapered stripline probe, with the water/FC-40 interface on top of the upper contact pad of the stripline chip. The capillary was connected at the bottom of the probe to a translation stage of the optical head of a DVD drive. This stage is moved by a stepper motor with a resolution of 160 μm per step (in our experiment we did two steps, so 320 μm, between each nutation experiment). The stepper motor and translation stage are magnetic and were therefore mounted to a plastic frame fixed to the bottom of the probe, separating motor and stripline by 120 cm. The stepper motor was controlled with an Arduino Uno, and a Python script was used to run the stepper motor and operate the software of the NMR machine, VnmrJ 3.2A, simultaneously. In total 83 steps were made and a total distance of 26.5 mm was analyzed. Processing of the nutation experiments and all other NMR experiments in this article were done using the Matlab based processing package matNMR [8]. For the nutation experiments the following parameters were used: 8 kHz spectral width, 160 ms acquisition time, 30 ms recycle delay, number of transients equal to 2 and a pulse width of 2.2 μs or multiples thereof, with a total of 320 increments.

The static imaging measurements were performed using a nutation experiment. Four silicone disks were measured using ^{1}H NMR at 144 MHz with tapered stripline chip 1 on a 3.4 T solid-state NMR (Oxford ultra-wide bore magnet, Varian Infinity Plus) system operated by Spinsight software. For the nutation experiment the following parameters were used: 40 kHz spectral width, 25 ms acquisition time, 3 s recycle delay, 4 scans per increment and a pulse width of 1.5 μs or multiples thereof, with a total of 300 increments.

The static measurement of the three liquid plugs was conducted by ^{1}H NMR at 600 MHz using tapered stripline chip 2 on a 14.1 T solid-state NMR (Oxford 600/89 magnet, Varian VnmrJ) system. For the nutation experiments the following parameters were used: 16 kHz spectral width, 1 s acquisition time, 9.5 s recycle delay, 16 scans per increment and a pulse width of 2.5 μs or multiples thereof, with a total of 300 increments.

The 1D nutation measurements on the three silicone rubber blocks were done with the same chip and NMR system. For the standard 2D arrayed nutation experiment the following parameters were used: 100 kHz spectral width, 50 ms acquisition time, 4 s recycle delay, 4 scans per increments and a pulse width of 2 μs or multiples thereof, with a total of 360 increments. For the 1D nutation experiment the following parameters were used: 25 kHz spectral width, 10 s recycle delay, 16 scans per increments, 40 μs per cycle, a pulse width of 2 μs and a total number of 360 acquired points.

For the experimental determination of the spatial resolution chip 3 was used on the 400 MHz Varian-Agilent system. A 10 cm long capillary was filled with H_2O and closed off on both sides with wax. The following parameters were used for the nutation experiment: 5 kHz spectral width, 1 s acquisition time, 2 s recycle delay, 1 scan per increment and a pulse width of 2.5 μs or multiples thereof, with a total of 1600 increments. During the entire experiment a B_0 gradient of 12.5 G/m was applied using the Z1 shim coil. The spatial resolution was determined by averaging the FWHM of the peak in the indirect dimension at 33 positions of the taper.

The reaction monitoring measurements were performed using ^{1}H NMR at 600 MHz with tapered stripline chip 2 on the 14.1 T solid-state NMR system. The liquids were pumped through the microfluidic system using gas-tight syringes and syringe pumps. The pumps were inside a fume hood and connected with 6 m long capillaries (250 μm ID) to union connectors on the bottom of the probe. From there on one liquid was directed through a 250 μm ID capillary and the other liquid through a 100 μm ID capillary. Both capillaries were connected to a T-connector on top of the probe. The 100 μm ID capillary was led all the way through the connector and into the outlet capillary (250 μm ID). Hereby we created a system in which the inner capillary contains liquid A and between the inner and the outer capillary there is liquid B. The end of the inner capillary was modified by Reith Laser (Wijchen, the Netherlands). The idea was to create a kind of micronozzle (Fig. S4), which should improve mixing, however we were only able to reduce the mixing time to a third of a second and besides that the mixer also caused some flow instability, for instance because gas bubbles built up inside the nozzle. The outlet capillary was positioned over the tapered stripline and exited the probe at the lower end (total length 1 m), were the reaction mixture was collected in a glass flask and the reaction was quenched with a sodium acetate solution in water. The micronozzle was positioned exactly on top of the narrowest side of the taper (Fig. S3) to be able to measure the mixture really from the start of the reaction.

The flow rates for DMF and $POCl_3$ were 9.0 and 3.0 μL/min respectively. Before the measurement started the system was allowed to stabilize for half an hour. A back pressure regulator was also tested to see if it stabilized the system, however, no positive effect was observed, instead the syringe pumps stalled more often and therefore the regulator was removed. The following parameters were used for the nutation experiment: 8 kHz spectral width, 1.5 s acquisition time, 3 s recycle delay, 1 scan per increment and a pulse width of 2 μs or multiples thereof, with a total of 256 increments.

The B_0 gradient compensation experiments were conducted on the 400 MHz NMR system, running ^{1}H NMR experiments in tapered stripline chip 3. The sample was a capillary filled with 1-propanol and a B_0 gradient was created by lowering the probe into the stray field of the NMR magnet. A pulse sequence based on the sequence with consecutive adiabatic full passages, described by Meriles et al. [9], was used. The adiabatic passages had a linear sweep that starts 1 MHz off resonance and has a maximum RF amplitude of 250 kHz. The length of the adiabatic half passage, used for an RF-independent excitation, was 150 μs and the full passages were 100 μs long. The total length of one block was 250 μs. The amplitude of the second full passage was 3.2% higher than the first passage for the largest B_0 gradient. The compensation experiments were recorded in a single scan with a sampling of 401 points at a rate of 4 points/ms. The amplitude of the second adiabatic full passage was incremented (with a 6 s recycle delay) to find the optimal adiabatic sweep amplitude. The methyl peak was set to 0.94 ppm (literature value for 1-propanol in $CDCl_3$).

3. Tapered stripline design

A typical configuration for a tapered stripline consists of five layers (Fig. 1): a central copper layer is electrolytically deposited on a fused silica substrate, which acts as an electrical insulator, these two layers together are the stripline chip. The chip is sandwiched between two copper ground planes. The bottom one is in direct contact with the fused silica, however, the top ground plane is separated from the central copper layer with Teflon spacers to ensure electrical insulation and to create space for the sample. The central copper layer is divided in three parts. The middle part

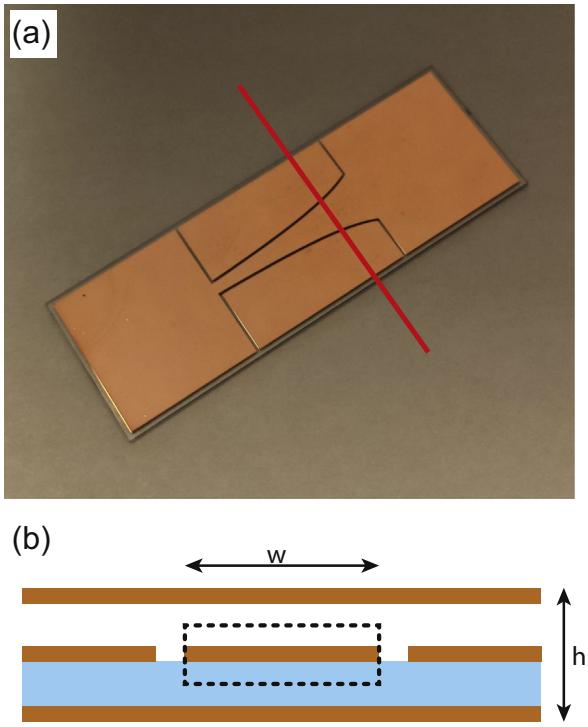

Fig. 1. (a) Picture of the tapered stripline chip (without copper ground planes) with a red line indicating the position of the cross section; (b) schematic cross section of the tapered stripline showing the copper parts (brown) and the fused silica substrate (blue). The dashed box shows Ampère's path, which can be used to determine the B_1 field strength. (For interpretation of the references to color in this figure legend, the reader is referred to the web version of this article.)

carries the current and generates the RF field, its width is varied over the length of the taper. The outer copper parts are not part of the electric circuit, but are in place for susceptibility matching.

The spectral resolution performance of striplines of constant width has been studied before [2,3]. The arguments presented there also apply to the present case. Because the plane in which the copper stripline is defined is extended with the copper outer parts one can approximate the B_0 field distortion induced by this plane using simple arguments based on Maxwell's equations. If the plane is oriented parallel to the field and if the contact pads are sufficiently long then the field will be nearly homogeneous along the sample volume probed by the stripline. There will be a small B_0 field offset, but in essence the gradient can be negligibly small and the resolution in the spatially resolved spectra remains uncompromised. In practice the main field distortion will be due to finite sample lengths and liquid or solid susceptibility plugs are needed.

The B_1 field strength on top of a stripline carrying a current I can be approximated using Ampère's circuital law:

$$\oint_C \vec{B}d\vec{s} = \mu_0 I \rightarrow B_1 \cong \frac{\mu_0 I}{2w+h} \quad (1)$$

where C is a closed rectangular path (dimensions: $w \times h/2$) around the central strip of the stripline, s is the infinitesimal in C, μ_0 is the magnetic permeability and w and h are the width of the confined part and height of the stripline chip, respectively. In this approximation we assumed that the B_1 field is parallel to the surface of the strip and nearly constant.

For imaging purposes, w has to be a function of the spatial coordinate, z, along the axis of the stripline. We can simplify

Eq. (1) further by eliminating the constants μ_0 and I. Also, there is a minimum B_1 field where the taper is at its widest:

$$b(z) \equiv \frac{1}{2(w(z)+d)} \tag{2}$$

$$b_{\min} \equiv \frac{1}{2(w_{\max}+d)} \tag{3}$$

where d is equal to $h/2$. In order to obtain a linear RF gradient over the stripline, $b/b_{\min}$ must be a linear function of z:

$$\frac{b(z)}{b_{\min}} = \frac{w_{\max}+d}{w(z)+d} = zG+1 \tag{4}$$

where G is the strength of the B_1 gradient. So it follows that for a stripline width profile:

$$w(z) = \frac{w_{\max}+d}{zG+1} - d \tag{5}$$

a normalized linear gradient in B_1 of strength G is generated. Fig. 2 shows plots of B_1 and w as functions of z. All tapered striplines in this manuscript were fabricated with the taper shape described by Eq. (5) to generate linear B_1 field gradients. However, in principle it is possible to fabricate a tapered stripline that can produce any desired gradient shape.

Since the detection sensitivity in NMR is proportional to the RF field strength per unit current [10], the sensitivity profile of the tapered stripline will have the same shape as the B_1 profile. So in quantitative measurements the data have to be corrected for this dependency, for example by using an internal reference. Here we present our data uncorrected for the local sensitivity profile, unless stated otherwise.

Besides detection, the excitation efficiency is also effected by the B_1 profile. Because of the B_1 gradient, the spins are excited with a spatial variation in the pulse angle. A uniform excitation can be achieved with an adiabatic passage.

4. Numerical verification of the RF profile

The RF pattern of the tapered stripline was numerically calculated for a taper with a length of 10 mm and a width described by Eq. (5) (tapered from 5 to 1 mm). Finite Element Method Magnetics (FEMM, a Matlab toolbox) was used to model a cross section of this tapered stripline and to calculate an approximate 2D RF field profile between the ground planes. This was done for 50 positions along the taper and these 2D RF field profiles were joined to produce a 3D profile. A current of 20 A was used for the central strip and the ground planes were set to −10 A.

The cross-sectional profile, Fig. 3a, shows large field distortions at the edges of the central strip, however, the B_1 field between the center of the central strip and the center of the ground planes is nearly homogeneous. For narrower sections of the tapered stripline an RF gradient will be present perpendicular to the strip. For those sections the plane of constant B_1 field will be curved, since there is both a gradient parallel and perpendicular to the strip. However, for wider sections of the tapered stripline this perpendicular gradient is negligible in size.

In Fig. 3b a cross section is shown parallel to the strip at half the height between the central strip and the ground plane. The figure shows that the tapered stripline generates a B_1 field that is homogeneous perpendicular to the axis of the taper and only deviates at the edges. For this slice the gradient field was calculated, Fig. 3c, and shown to be constant over the entire length of the taper. Again only the edges show a deviation from the tapers RF gradient strength.

5. Experimental verification of the RF profile

We characterized the RF field profile experimentally by displacing a water/FC-40 interface stepwise over the taper and performing a nutation experiment every 320 μm. At zero displacement only FC-40, which is a proton-free perfluorocarbon mixture, was on top of the taper and the water was on top of one of the broad connection pads on the chip. As the water/FC-40 interface was moved over the chip, a larger section of the taper was covered by water. Each nutation experiment then gave an RF profile, which tells us what RF field strengths were felt by the water sample. By subtracting each RF profile from the preceding one we can determine the RF field for a 320 μm long section of the tapered stripline. In total 83 displacements were executed, giving the full RF field profile of the tapered stripline (Fig. 4). As expected the tapered stripline gives a nearly perfect linear RF field profile. The field has a steep transition (at 7 mm displacement) going from the broad contact pads of the chip to the narrowest side of the taper and the field at the contact pads is, with 18 kHz, relatively low.

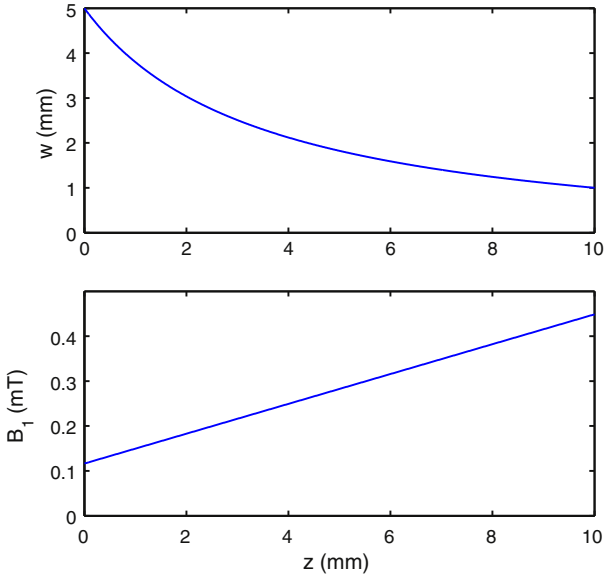

Fig. 2. Plots of the stripline width w (top) and the corresponding linear B_1 field (bottom) as a function of the position. G is chosen such that the $w_{max}/w_{min} = 5$ for a 10 mm long taper, $h = 800$ μm, $I = 1$ A.

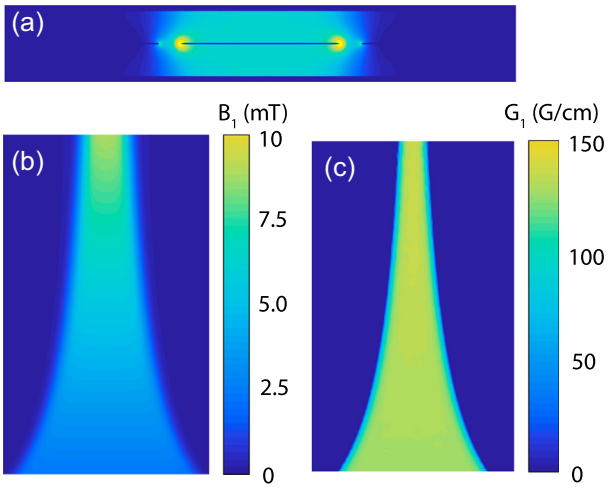

Fig. 3. (a) B_1 field of a cross section of the tapered stripline, taken at the middle of the taper. (b) B_1 field halfway between the center strip and the top ground plane. (c) B_1 gradient strength at the same height as figure (b).

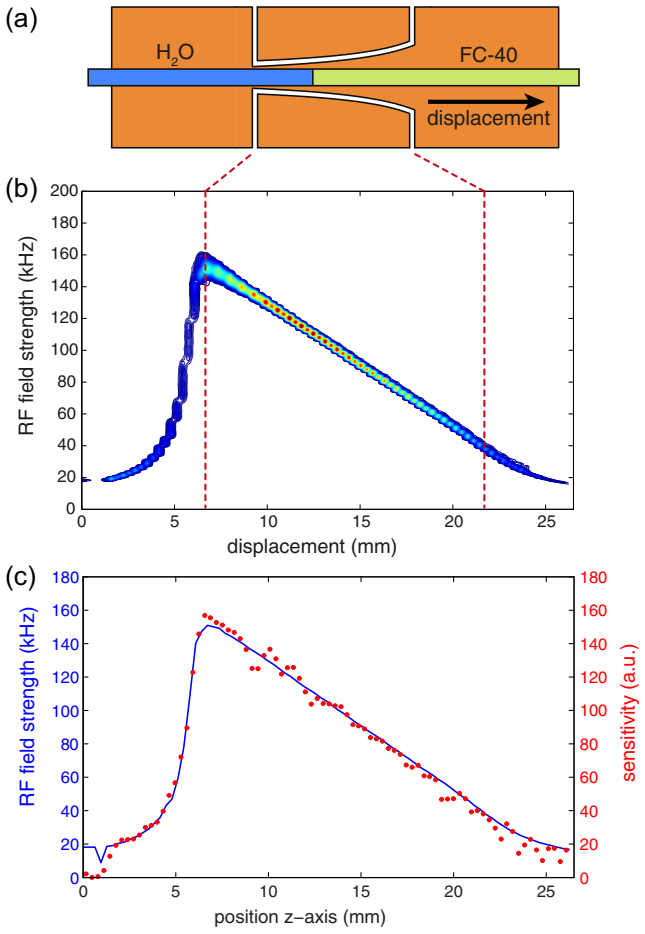

Fig. 4. RF mapping of the tapered stripline: (a) sketch of how the sample capillary is moved over the tapered stripline; (b) a contour plot of the raw data which displays the RF field distribution along the tapered stripline in 83 discrete steps of 320 μm; (c) the tapered stripline's RF field strength (blue) and sensitivity (red) as a function of the position on the *z*-axis. The tapered stripline chip has a 15 mm long taper with a width that changes from 1 to 5 mm. (For interpretation of the references to color in this figure legend, the reader is referred to the web version of this article.)

From the same data we could extract the sensitivity profile of the tapered stripline (Fig. 4c) by integrating the peak in the direction of the RF field strength. This first resulted in a modulated profile, because the steps of the stepper motor were not exactly equal in size. However, they were periodic, so averaging of the neighboring data points resulted in a smooth profile. As expected from the reciprocity theorem, the sensitivity profile of the tapered stripline is equal to the RF field profile. This means that for quantitative measurements the results have to be corrected with the experimental profile of Fig. 4c, or one can also simply make use of an internal standard. The sensitivity profile deviates from the RF profile at very low and high displacements. The deviation at low displacements can be explained by the fact that after connecting the sample capillary to the stepper motor, the capillary is not yet under tension and the water/FC-40 interface does not move. The RF profile measured in the consecutive nutation experiments is thus the same. Subtracting the profiles results therefore in zero intensity.

The RF field profile can also be determined with the help of a static linear B_0 gradient, where the resonance frequency encodes for position [11]. Then in a single nutation experiment the full RF field profile can be obtained. However, in that case the initial shimming, the linearity of the applied B_0 field and uniformity of the sample all have to be perfect. Because the measurement of the RF profile only has to be done once to verify the design concepts, we prefer the longer method, in which no assumptions have to be made.

The same tapered stripline chip was used to determine the maximum gradient strength. The proton amplifier was set to maximum power (450 W) and a nutation experiment was performed. A maximum RF field of 630 kHz was observed with a field difference of roughly 350 kHz over the 15 mm length of the taper, which is equivalent to a gradient strength of 55 G/cm. This is on the same order as the B_0 gradients in standard liquid-state probes, which range from 50 to 100 G/cm. However, nowadays specialized diffusion probes are commercially available with pulsed gradients that are an order of magnitude stronger (1000–3000 G/cm). Nevertheless, 55 G/cm is a decent gradient strength and some small modifications to the chip, for instance a reduction in the length of the taper, should allow us to reach B_1 field gradients of more than 100 G/cm.

6. Imaging of static samples

The RF gradient of the tapered stripline can be used for static imaging experiments. The spatial information is encoded during the excitation pulse as an RF-dependent phase. The RF frequencies can be determined from a nutation experiment. After a Fourier transform in both the direct and indirect dimension the data obtained are a 1D-image in the F_1 dimension, whereas the spectral information is contained in the F_2 dimension. A more extensive description of this B_1 imaging method and the processing is given in the Supplementary information.

The imaging capability of the tapered stripline chip was first tested on a set of disks. Four silicone rubber disks with a diameter of 250 μm were placed 2 mm apart in a straight line along the axis of the tapered stripline and a nutation experiments was performed. The image (Fig. 5) clearly visualizes the capability of our method to map the distinct positions of the silicone disks. The peaks in the skyline plot (F_1 dimension) are 3.6 kHz wide, corresponding to a spatial width of 273 μm, which is in good agreement with the diameter (250 μm) of the silicone rubber disks. In the F_2 dimension we observe one narrow peak from the rapidly rotating methyl group in the silicone rubber.

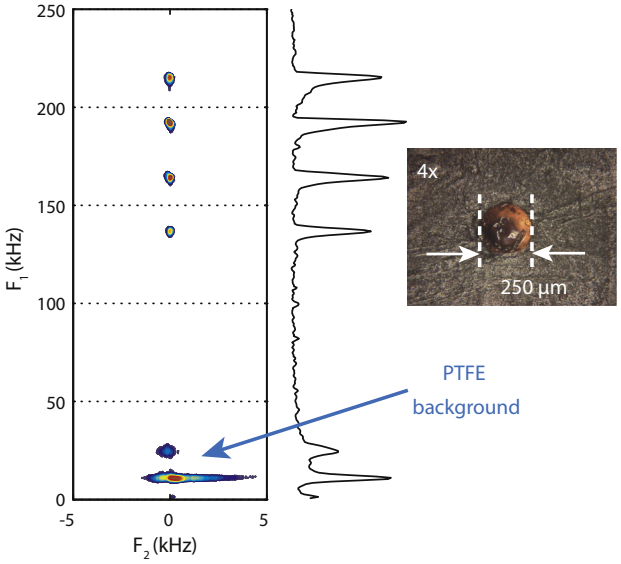

Fig. 5. 1D-image (contour plot) of four small silicone rubber disks (250 μm diameter, 200 μm height), made by filling holes in a PTFE substrate. 300 increments, t_{exp} = 1 h. Background signal from the PTFE substrate is effectively sorted out, since it experiences a lower RF field. On the right a skyline projection is shown.

In general a single nutation experiment in combination with the tapered stripline gives a 1D-image of the sample, but it also contains all the chemical shift information, thus it gives both spatial and spectral information. To demonstrate that the chemical shift information is preserved, another measurement was performed. A capillary was filled with three plugs of different compounds, each separated by FC-40, as displayed in Fig. 6. From these data, the position as well as the chemical composition of the sample plugs could be deduced straightforwardly. The spectra that were taken from the image show that the spectral resolution is good.

If one is only interested in the spatial information and not in the spectral information, then the nutation experiment can be performed in a single 1D experiment [12,13] instead of a 2D array. A train of equal pulses is given and the acquisition is done by sampling a single data point between each pulse pair. The resulting FID gives a nutation spectrum, and thus a 1D image, after a single Fourier transformation. With this method one does not have to run an array and can reduce the experimental time by a factor of several hundred (depending on the number of points and the desired signal to noise ratio). We tested the method on three silicone rubber blocks (Fig. 7) and found minimal differences between the results of the standard 2D arrayed nutation and the 1D nutation.

7. Spatial resolution

The theoretical spatial resolution of this imaging method is – analogous to the resolution in the spectral dimension – determined by the length of the recorded signal. In the spatial dimension this is equivalent to the longest pulse in the nutation experiment, which is limited by the bandwidth that has to be excited. For example, if protons are observed at 600 MHz in a bandwidth of 10 ppm (6 kHz), then the maximum pulse width allowable is 1/(6 kHz) = 167 μs. This limit on the resolution arises from the need to have a pulse that is uniformly effective over the entire range of Larmor frequencies of the sample. If the maximum pulse width is 167 μs,

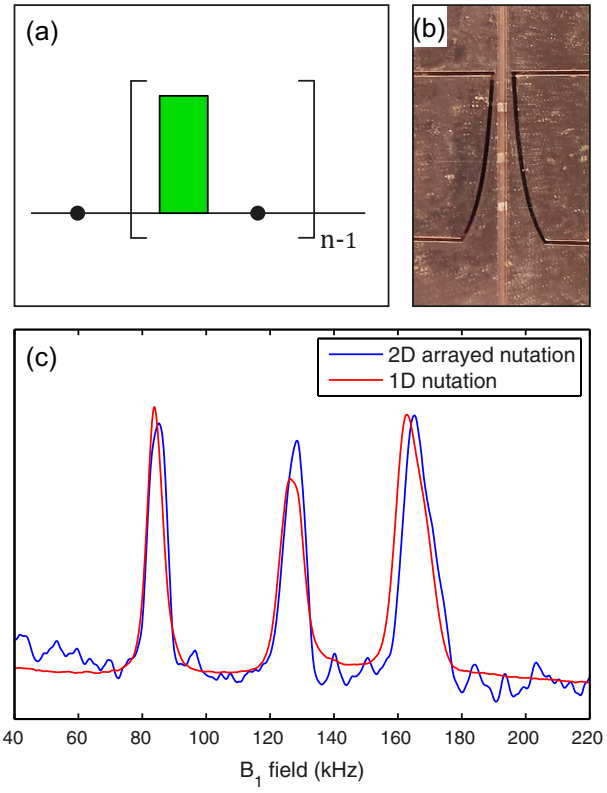

Fig. 7. (a) The 1D nutation pulse sequence, *n* points are acquired and between each point the magnetization is further nutated by a pulse; (b) three silicone rubber blocks on top of the tapered stripline; (c) nutation spectra of the three silicone rubber blocks. The spectra were acquired with 360 increments (4 scans per increment) for the 2D nutation and 360 points (16 scans per point) for the 1D nutation. In the 2D nutation the pulse length was incremented by 2 μs and in the 1D nutation experiment 2 μs pulses were used.

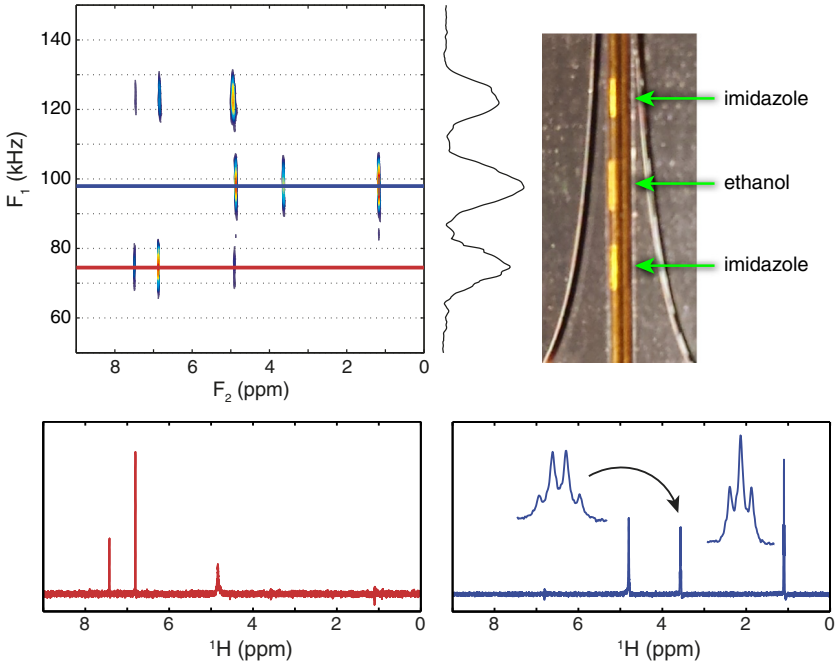

Fig. 6. Imaging of three liquid plugs, separated by FC-40. All liquids are dissolved in D_2O up to a 2 M concentration. The top and bottom plugs are imidazole (6.9 and 7.5 ppm) and the middle one is ethanol (1.2, 3.6 and 4.9 ppm). Top left: The ^1H image of the three droplets. Bottom left and right: spectra taken from the image at positions indicated by the red and blue horizontal lines. Top right: a picture of the tapered stripline chip with liquid plugs inside the capillary. The photo was taken under an angle, such that the reflection of the light gave a clear contrast between the droplets and FC-40. (For interpretation of the references to color in this figure legend, the reader is referred to the web version of this article.)

then the resolution in the indirect dimension is 1/(167 μs) = 6 kHz. Since the shape of the RF field gradient is linear, the resolution in the indirect dimension ($R_{indirect}$) can be directly converted by Eq. (6) into the resolution of the spatial dimension ($R_{spatial}$) if the length of the taper (L_{taper}) and the RF field at the narrowest (RF_{max}) and widest (RF_{min}) part of the taper, or the RF gradient (G_{RF}) are known.

$$R_{spatial} = \frac{L_{taper} \cdot R_{indirect}}{RF_{max} - RF_{min}} = \frac{R_{indirect}}{G_{RF}} \quad (6)$$

For solid-state samples the spatial resolution can be limited by the spectral line width (T_2). For instance if the peaks are 10 kHz wide in the direct dimension due to dipolar broadening, then these peaks are at least 10 kHz broad in the indirect dimension (which is proportional to the spatial dimension). One can stretch this limit by moving to nutation experiments with higher RF fields.

If one is not interested in the spectral information, but only in the spatial distribution of a certain compound, then the spatial resolution is no longer limited by the bandwidth. Instead it is limited by the practical limit of the pulse length (to prevent RF heating and arcing) and the sensitivity of the probe. The voxel should be large enough so that it contains at least the number of spins necessary to give a detectable signal in a reasonable amount of time. For example, for a ^{1}H image of water in a capillary (250 μm ID), recorded with a receiver bandwidth of 5 kHz, a S/N of 5 in the FID (single scan) and a sensitivity of 10^{14} spins/$\sqrt{}$Hz the spatial resolution is 10 μm.

Eq. (6) shows that the spatial resolution can be optimized by matching the length of the taper to the length of the sample and by maximizing the RF gradient. The latter can be achieved by moving to higher RF pulse powers, which is again limited for practical reasons, or to more strongly tapered striplines (higher w_{max}/w_{min}), i.e. making the narrow end of the taper more narrow. However, in this case the shape of the voxel will change. If the stripline is wide, the magnetic field lines are confined between the two ground planes and give a very homogeneous B_1 field, with only inhomogeneous sections close to the sides of the central strip. However, for a narrow stripline the sample volume extends into the inhomogeneous region and there is not only a B_1 field gradient parallel to the taper, but also one perpendicular to the plane of the chip, with a high field strength close to the central strip and a weaker field strength close to the ground planes. As a consequence the slice of equal RF field is no longer flat and perpendicular to the taper, instead it is curved and compromises the resolution. In principle one can account for this and do a reconstruction.

Finally, in low viscosity media the resolution may also be limited by diffusion. However, this effect is nearly negligible: a water molecule at room temperature diffuses only 2 μm on average during a 1 ms pulse.

The practical spatial resolution of the current design was determined experimentally by performing a 2D nutation experiment on a 50 μm (ID) capillary filled with H_2O, while applying a small B_0 gradient of 12.5 G/m by adjusting the Z1 shim. The B_0 gradient basically divides the water sample in infinitesimal fractions, each with their own Larmor frequency, so in the nutation image this gives a long diagonal peak. By measuring the FWHM of this peak in the indirect dimension (F_1) the spatial resolution can be determined. We determined the FWHM at several positions along this peak and found an average spatial resolution of approximately 100 μm, or approximate voxel volumes of 200 pL.

8. Reaction monitoring

Bart et al. [2] showed that the stripline design can be used to monitor reactions in a flow NMR setup. Many other flow NMR systems have been described in literature. Most of them use high magnetic fields and only make minor adjustments to the standard liquid-state NMR probes [14–17]. In recent years several excellent benchtop NMR machines have entered the market, with very homogeneous fields that are stable over longer periods. This has literally brought the NMR machine inside the fume hood and has already given several good examples of low-field NMR reaction monitoring [18–21]. However, there are few examples of flow NMR systems [22] in which the hardware is adapted to very low detection volumes (on the order of a few microliters down to several picoliters) that match those of a microfluidic system. Microfluidic systems are used in microreactor synthesis, the production of microdroplets for biochemistry and several other fields. They offer many advantages over traditional systems [21–26] including perfect control over temperature and reaction time, less solvent and good safety control. So they make it possible to study more violent and fast reactions.

The next challenge in flow NMR is to be able to monitor fast chemical reactions. Reactions of a few seconds or less are difficult to monitor with high spectral resolution because the acquisition length is on the same time scale, although ultrafast 2D NMR techniques [27,28] have made it possible to obtain more information on this short time scale. Up to now, sub-second reactions can only be monitored with stopped-flow and rapid injection NMR techniques [29–31], however, these methods are laborious. Our tapered stripline setup is optimized for the small sample volumes of microfluidic systems and by applying the nutation sequence to a continuous flowing reaction mixture (with a fixed flow rate) we should be able to produce a kinetic profile of the reaction, in the same way as we would get a one-dimensional image of a static sample.

We tested our method on the first step of the Vilsmeier–Haack reaction, which was discovered in 1927 as a new way to functionalize an electron-rich aromatic ring with an aldehyde [32]. This so-called formylation reaction consists of three steps: the formation of the extremely reactive iminium ion, also called the Vilsmeier reagent; the reaction of an electron-rich arene with this reagent

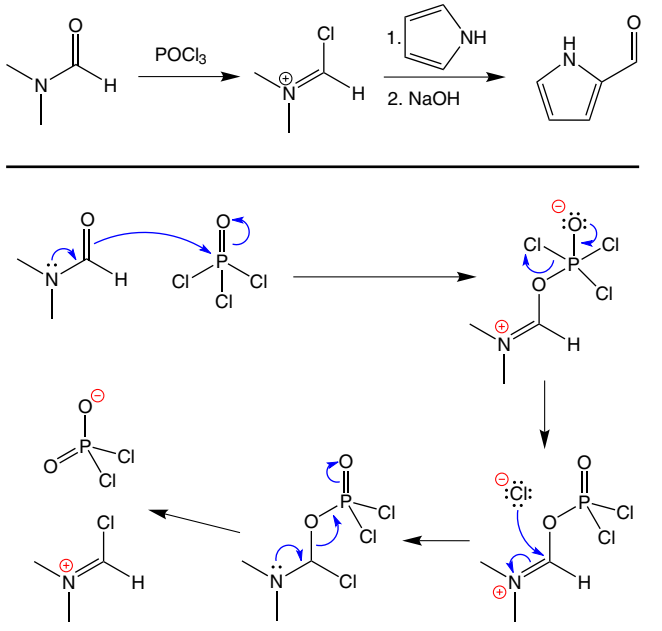

Fig. 8. Reaction scheme for the Vilsmeier–Haack reaction. Top: overview of the full reaction. DMF reacts with $POCl_3$ and forms the Vilsmeier reagent, this is then used in two consecutive steps to formylate an electron-rich aromatic ring (in this case pyrrole). Bottom: the proposed mechanistic scheme of the formation of the Vilsmeier reagent.

and an aqueous work-up step (Fig. 8). In the first step N,N-dimethylformamide (DMF) reacts with phosphoryl chloride ($POCl_3$). Via several intermediates the oxygen atom of the DMF gets exchanged for a chlorine atom and an iminium ion ($R_2C{=}N^+R_2$) is formed. Note that the C(=O)—N bond has a double bond character [33], therefore, the DMF and all intermediates can have two peaks for the methyl groups.

The reaction, in particular the first step, is very fast and exothermic and serious thermal hazards have been reported [34]. The safety risks can be brought to a minimum by using a microfluidic flow setup instead of the standard reaction flask.

9. Experimental results reaction monitoring

The reaction monitoring setup described in the experimental section was used to study the first step in the Vilsmeier–Haack reaction: the formation of the iminium ion. It was already known from literature that this step would be fast (completed within 90 s in a solution of acetonitrile [35]). Using our method we monitored the first 2.5 s of the reaction of the pure compounds.

A problem we encountered was the mixing of the liquids. At the small length scales in the capillary and the slow flow rates the flow is no longer turbulent, instead there is a laminar flow. So mixing occurs only on the basis of diffusion, which is too slow to study the fast reaction kinetics. We tried to overcome this problem by using a micro nozzle, as described in the experimental section. This did improve mixing, but not enough to obtain fully quantitative kinetic information.

Nevertheless, this method can still give extremely valuable information about the reaction mechanism. The spectra of the Vilsmeier–Haack reaction, Fig. 9, give detailed information of the first 1.5 s of the reaction. At $t = 0$ s three peaks are observed, corresponding to the methyl groups (2.88 and 3.05 ppm) and N—H group (8.13 ppm) of DMF. These lines quickly broaden in an asymmetric way in the upfield direction and keep this shape for 20 s (as was determined with the method of Oosthoek-de Vries et al. [7]). This can be explained partly by incomplete mixing, but most likely it indicates the dynamic formation of one of the intermediates. Additional broadening may be caused by intramolecular chemical exchange, namely the hindered rotation around the C(=O)—N or C(—Cl)—N bonds, and by intermolecular chemical exchange (for instance the addition and reduction of a chlorine atom to the positively charged intermediate).

After a few hundred milliseconds peaks emerge (3.38, 3.54 and 9.46 ppm) of what we assume to be the Vilsmeier reagent. Remarkably these peaks also have an asymmetric shape, only with a broadening in the downfield direction.

From the 2D matrix we integrated the DMF peaks and the peaks of the Vilsmeier reagent and the possible intermediates. The signal intensity along the taper is scaled according to the sensitivity profile of the tapered stripline (Fig. 4), therefore the conversion (Fig. 10) was calculated by dividing the signal of the Vilsmeier reagent and the intermediates by the integral of the full spectrum.

The reaction does not reach 100% conversion because an excess of DMF (3:1 v/v) was used to keep the viscosity of the reaction mixture low, so the curve levels off to the theoretical maximum conversion at 27.7%.

Our reaction monitoring method shows some very interesting changes in the reaction mixture of the Vilsmeier–Haack reaction at short reaction times on the order of several hundreds of milliseconds. However, slower processes are also present and after a long reaction time the NMR spectrum shows more changes, i.e. narrowing of the methyl peaks and formation of several side products. The Vilsmeier–Haack reaction is clearly a very complex reaction and more research has to be done to fully understand the mechanism and to assign all the peaks. In the present context it is not possible to give a full, detailed description of this reaction. However, these preliminary results underline the potential of our method to study chemical processes at a time scale of tens of milliseconds up to several seconds.

10. B_0 gradient compensation

As a third application example for the tapered stripline approach we will discuss the possibility for arbitrary B_0 gradient compensation.

Between 2000 and 2005 the Pines group published a series of papers [9,36–39] in which they describe how B_1 field gradients can be used to retrieve spectral resolution in inhomogeneous magnetic (B_0) fields. Their methods can be used in portable single-sided NMR systems or in other systems where perfect B_0 homogeneity is impossible to realize using standard shimming techniques.

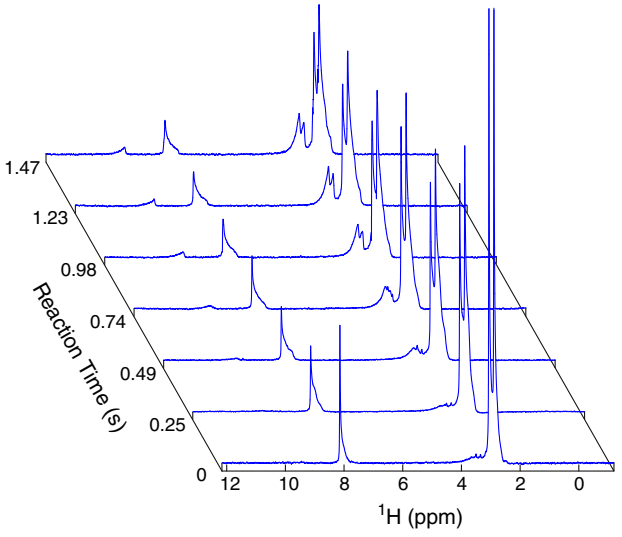

Fig. 9. Spectra of the Vilsmeier–Haack reaction, showing the methyl region at different reaction times. The most upfield peak at 0 s was set to 2.88 ppm (the literature value for DMF in $CDCl_3$). The spectra are corrected for the sensitivity profile of the tapered stripline.

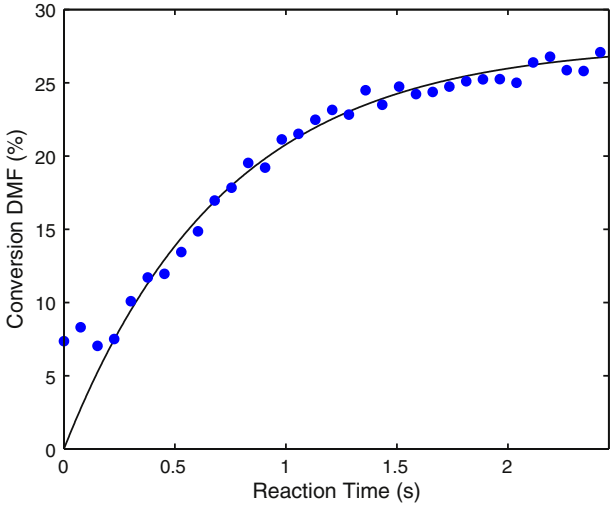

Fig. 10. Conversion of dimethylformamide in the first step of the Vilsmeier–Haack reaction. The flow rates are 9 μL/min for DMF and 3 μL/min for $POCl_3$. The conversion was calculated from a nutation measurement with 256 increments (1 scan each), acquired in a total time of 20 min.

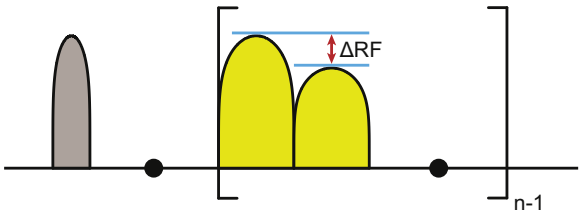

Fig. 11. Pulse sequence for obtaining B_0 gradient compensated spectra: after an adiabatic half passage (gray) a windowed acquisition is started. Between the acquisition points (black dots) sets of two adiabatic full passages (yellow) are given. The amplitude of the second adiabatic passage is optimized such that phase produced by the double passage matches the phase introduced by the B_0 field gradient. (For interpretation of the references to color in this figure legend, the reader is referred to the web version of this article.)

In an inhomogeneous field a phase shift of the local magnetization is needed to compensate for the difference in Larmor precession due to the B_0 variations over the sample. The Pines group first used composite z-rotation pulses to create this position dependent phase shift [36,37], but later they switched to consecutive adiabatic passages [9,38,39], because these are more effective over a large bandwidth. Since our tapered stripline produces a linear B_1 profile we are able to obtain spectrally resolved NMR spectra in the presence of linear B_0 field variations using the method of the Pines group. However, as the tapered stripline offers the advantage of perfect control over the shape of the B_1 field gradient, any B_0 field profile can be compensated for.

The pulse sequence (Fig. 11) we used is very similar to the one used by the Pines group. An adiabatic half passage is used to create transverse magnetization. Then a windowed acquisition is started in which between every two acquisition points a set of two adiabatic full passages is used to compensate the dephasing due to the B_0 field gradient. In an adiabatic passage the angle between the magnetization vector and the effective field is maintained. However, depending on the resonance offset and the RF field strength a phase develops during the passage. So the first adiabatic full passage introduces a phase, as a function of both the local RF field strength and the offset. A second identical adiabatic passage will cancel this introduced phase. However, because the second passage has a different RF amplitude there will be a residual phase that is only dependent on the difference in RF field strength. So the amplitude of the second adiabatic passage can be optimized such that the phase produced by the double passage matches and thus cancels the phase introduced by the B_0 field gradient during free evolution.

11. Experimental results B_0 gradient compensation

The B_0 gradient compensation pulse sequence was tested at three positions in the magnet: the homogeneous center, a slightly inhomogeneous part (13 G/m) and deeper in the stray field of the magnet (172 G/m). Fig. 12 displays the spectra obtained at these three positions with both a single 90° pulse and with the B_0 gradient compensation pulse sequence. Clear differences are visible in the spectra acquired in the homogeneous center of the magnet. The apparent J-coupling is larger in the spectrum obtained with the compensation pulse sequence. In fact the J-coupling has remained the same, but the chemical shift is scaled. In this pulse sequence the chemical shift only evolves during the time between the sets of adiabatic full passages. The J-coupling, on the other hand, is unaffected by the adiabatic sweeps and is active during the entire windowed acquisition. For the measurements in Fig. 12 the compensation sequence was run with 100 μs long adiabatic full passages and a point-by-point acquisition of 1 point per 250 μs. So the chemical shift evolves only 50 μs between each point and the chemical shift is thus scaled by a factor 5.

Under a small B_0 gradient of 13 G/m the spectrum looks very crowded, however, the compensation pulse sequence is able to fully recover the spectral resolution. At a larger gradient of 172 G/m the lines in the standard 1D spectrum are broadened so much that they fully overlap and the resulting spectrum consists of only a single broad peak. With the compensation pulse sequence it is still possible to recover most of the spectral information and to distinguish the five peaks. However, the peaks are broadened and

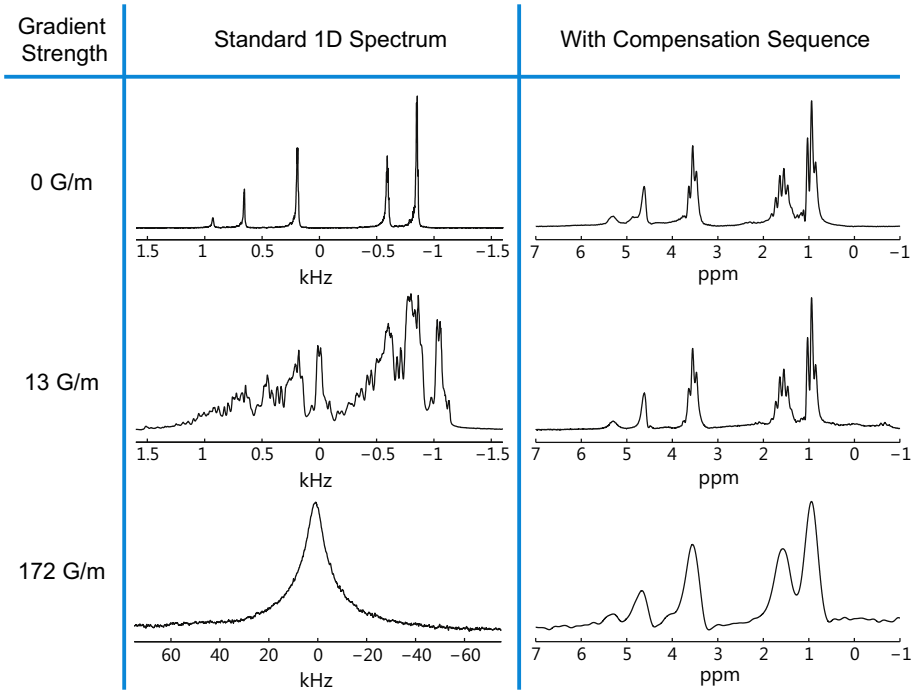

Fig. 12. Spectra of 1-propanol. The top spectra were acquired in the homogeneous part of the magnet. The middle and bottom spectra were acquired in the stray field of the magnet. The spectra on the left are simple 1D spectra, acquired after a single 90° pulse. The spectra on the right are acquired with the B_0 compensation sequence.

the triplets and multiplet are no longer visible. This can be explained by the shape of the stray field of the magnet, which is used to create the magnetic field gradient. For a small section of the stray field the gradient is approximately linear, but as the gradient becomes larger this approximation no longer holds. In that case our tapered stripline, with its linear gradient, does not perfectly match the B_0 field gradient anymore.

12. Conclusions and outlook

The constriction in a stripline NMR detector can be shaped such that a linear B_1 gradient is obtained. This tapered stripline can be used for 1D imaging and may offer several advantages over imaging with B_0 gradients. Furthermore in this approach the chemical shift information is completely preserved. We have shown the applicability of the tapered stripline by monitoring the first 2.5 s of the Vilsmeier–Haack reaction in a microfluidic tapered stripline chip. Hereby we demonstrated that it is possible to study reactions by NMR on a time scale on the order of hundreds of milliseconds up to several seconds. The combination of flow chemistry and tapered stripline NMR is in principle a very promising one. Flow chemistry allows one to perform reactions in a very controlled manner and with perfect control over timing and temperature, bringing the exploration of more exotic reactions, which were previously regarded as too dangerous or difficult to perform, within reach. Stripline NMR offers all the advantages of NMR and sensitivity-wise the stripline design is the preferred choice to match the nL–μL sample volumes in microfluidics. Future research should be aimed at a better integration of the microfluidic system into the probe, and at improved mixing to obtain quantitative data to allow analysis of the pure reaction kinetics.

As a final application we showed that the tapered stripline can be used to compensate B_0 gradients and retrieve the spectral resolution obtained in homogeneous fields. In principle the shape of the tapered stripline can be modified to create any desired RF field profile. So one could use a tapered stripline with a linear gradient to map the B_0 field profile, and from that profile design a stripline chip with a B_1 field profile that matches the B_0 field profile. This stripline can then be used to obtain high resolution spectra in inhomogeneous B_0 fields.

Another obvious extension of the tapered stripline is the measurement of spatial diffusion in microfluidic systems. Work in this direction is ongoing.

Because stripline chips are flat and easily scalable, it is possible to apply them in benchtop spectrometers or even smaller miniaturized NMR systems [40,41]. These systems are relatively sensitive and low in cost, which makes them ideal for medical and industrial applications.

Acknowledgments

This work is financed by the Institute for Molecules and Materials (IMM) of the Radboud University and by Netherlands Organization for Scientific Research (NWO). The authors would like to thank the staff of Future Chemistry (Nijmegen, The Netherlands) for their help in the study of the Vilsmeier–Haack reaction and their help in building a microfluidic setup. The authors would like acknowledge Bas van Meerten (ss-NMR group, Radboud University) for his contributions in the experimental verification of the RF field profile of the tapered stripline.

Appendix A. Supplementary data

Supplementary data associated with this article can be found, in the online version, at http://dx.doi.org/10.1016/j.jmr.2015.12.021.

References

[1] A.P.M. Kentgens, J. Bart, P.J.M. van Bentum, A. Brinkmann, E.R.H. van Eck, J.G.E. Gardeniers, J.W.G. Janssen, P. Knijn, S. Vasa, M.H.W. Verkuijlen, High-resolution liquid- and solid-state nuclear magnetic resonance of nanoliter sample volumes using microcoil detectors, J. Chem. Phys. 128 (2008) 052202.
[2] J. Bart, J.W.G. Janssen, P.J.M. van Bentum, A.P.M. Kentgens, J.G.E. Gardeniers, Optimization of stripline-based microfluidic chips for high-resolution NMR, J. Magn. Reson. 201 (2) (2009) 175–185.
[3] P.J.M. van Bentum, J.W.G. Janssen, A.P.M. Kentgens, J. Bart, J.G.E. Gardeniers, Stripline probes for nuclear magnetic resonance, J. Magn. Reson. 189 (1) (2007) 104–113.
[4] D.I. Hoult, Rotating frame zeugmatography, J. Magn. Reson. 33 (1) (1979) 183–197.
[5] P. Maffei, P. Mutzenhardt, A. Retournard, B. Diter, R. Raulet, J. Brondeau, D. Canet, NMR microscopy by radiofrequency field gradients, J. Magn. Reson., Ser. A 107 (1) (1994) 40–49.
[6] J. Bart, A.J. Kolkman, A.-J. Oosthoek-de Vries, K. Koch, P.J. Nieuwland, J.W.G. Janssen, P.J.M. van Bentum, K.A.M. Ampt, F.P.J.T. Rutjes, S.S. Wijmenga, J.G.E. Gardeniers, A.P.M. Kentgens, A microfluidic high-resolution NMR flow probe, J. Am. Chem. Soc. 131 (14) (2009) 5014–5015.
[7] A.-J. Oosthoek-de Vries, J. Bart, R.M. Tiggelaar, J.W.G. Janssen, P.J.M. van Bentum, J.G.E. Gardeniers, A.P.M. Kentgens, Continuous flow ^{1}H and ^{13}C NMR spectroscopy in microfluidic stripline NMR chips, Anal. Chem. (submitted for publication).
[8] J.D. van Beek, MatNMR: a flexible toolbox for processing, analyzing and visualizing magnetic resonance data in Matlab, J. Magn. Reson. 187 (1) (2007) 19–26.
[9] C.A. Meriles, D. Sakellariou, A. Pines, Broadband phase modulation by adiabatic pulses, J. Magn. Reson. 164 (1) (2003) 177–181.
[10] D.I. Hoult, R.E. Richards, The signal-to-noise ratio of the nuclear magnetic resonance experiment, J. Magn. Reson. 24 (1) (1976) 71–85.
[11] A. Bax, Two-Dimensional Nuclear Magnetic Resonance in Liquids, Delft University Press, D. Reidel Publishing Company, 1982, pp. 22–26.
[12] P.S.C. Wu, G. Otting, Rapid pulse length determination in high-resolution NMR, J. Magn. Reson. 176 (1) (2005) 115–119.
[13] D. Horne, R.D. Kendrick, C.S. Yannoni, Bond length measurements in amorphous solids by nutation NMR spectroscopy: the role of rf field homogeneity, J. Magn. Reson. 52 (2) (1983) 299–304.
[14] M. Maiwald, H.H. Fischer, Y.-K. Kim, K. Albert, H. Hasse, Quantitative high-resolution on-line NMR spectroscopy in reaction and process monitoring, J. Magn. Reson. 166 (2) (2004) 135–146.
[15] M.A. Bernstein, M. Štefinović, C.J. Sleigh, Optimising reaction performance in the pharmaceutical industry by monitoring with NMR, Magn. Reson. Chem. 45 (7) (2007) 564–571.
[16] D.A. Foley, E. Bez, A. Codina, K.L. Colson, M. Fey, R. Krull, D. Piroli, M.T. Zell, B.L. Marquez, NMR flow tube for online NMR reaction monitoring, Anal. Chem. 86 (24) (2014) 12008–12013.
[17] Y. Takahashi, M. Nakakoshi, S. Sakurai, Y. Akiyama, H. Suematsu, H. Utsumi, T. Kitamori, Development of an NMR interface microchip "MICCS" for direct detection of reaction products and intermediates of micro-syntheses using a "MICCS-NMR", Anal. Sci. 23 (4) (2007) 395–400.
[18] N. Zientek, C. Laurain, K. Meyer, M. Kraume, G. Guthausen, M. Maiwald, Simultaneous ^{19}F–^{1}H medium resolution NMR spectroscopy for online reaction monitoring, J. Magn. Reson. 249 (2014) 53–62.
[19] M.V. Silva Elipe, R.R. Milburn, Monitoring chemical reactions by low-field benchtop NMR at 45 MHz: pros and cons, Magn. Reson. Chem. (2015) (Epub ahead of print).
[20] V. Sans, L. Porwol, V. Dragone, L. Cronin, A self optimizing synthetic organic reactor system using real-time in-line NMR spectroscopy, Chem. Sci. 6 (2015) 1258–1264.
[21] E. Danieli, J. Perlo, A.L.L. Duchateau, G.K.M. Verzijl, V.M. Litvinov, B. Blümich, F. Casanova, On-line monitoring of chemical reactions by using bench-top nuclear magnetic resonance spectroscopy, ChemPhysChem 15 (14) (2014) 3060–3066.
[22] A. Scheithauer, A. Brächer, T. Grützner, D. Zollinger, W.R. Thiel, E. von Harbou, H. Hasse, Online ^{1}H NMR spectroscopic study of the reaction kinetics in mixtures of acetaldehyde and water using a new microreactor probe head, Ind. Eng. Chem. Res. 53 (45) (2014) 17589–17596.
[23] D.T. McQuade, P.H. Seeberger, Applying flow chemistry: methods, materials, and multistep synthesis, J. Org. Chem. 78 (13) (2013) 6384–6389.
[24] I.R. Baxendale, L. Brocken, C.J. Mallia, Flow chemistry approaches directed at improving chemical synthesis, Green Process. Synth. 2 (3) (2013) 211–230.
[25] J. Yoshida, A. Nagaki, T. Yamada, Flash chemistry: fast chemical synthesis by using microreactors, Chem. Eur. J. 14 (25) (2008) 7450–7459.
[26] J. Yoshida, Flash Chemistry: Fast Organic Synthesis in Microsystems, Wiley, 2008.
[27] P. Giraudeau, L. Frydman, Ultrafast 2D NMR: an emerging tool in analytical spectroscopy, Annu. Rev. Anal. Chem. 7 (2014) 129–161.
[28] M. Mishkovsky, L. Frydman, Principles and progress in ultrafast multidimensional nuclear magnetic resonance, Annu. Rev. Phys. Chem. 60 (2009) 429–448.
[29] R.O. Kühne, T. Schaffhauser, A. Wokaun, R.R. Ernst, Study of transient chemical reactions by NMR. Fast stopped-flow Fourier transform experiments, J. Magn. Reson. 35 (1) (1979) 35–67.

[30] M.D. Christianson, E.H.P. Tan, C.R. Landis, Stopped-flow NMR: Determining the kinetics of [*rac*-(C_2H_4(1-indenyl)$_2$)ZrMe][MeB(C_6F_5)$_3$]-catalyzed polymerization of 1-hexene by direct observation, J. Am. Chem. Soc. 132 (33) (2010) 11461–11463.
[31] M. Kakuta, D.A. Jayawickrama, A.M. Wolters, A. Manz, J.V. Sweedler, Micromixer-based time-resolved NMR: applications to ubiquitin protein conformation, Anal. Chem. 75 (4) (2003) 956–960.
[32] A. Vilsmeier, A. Haack, Über die Einwirkung von Halogenphosphor auf Alkyl-formanilide. Eine neue Methode zur Darstellung sekundärer und tertiärer p-Alkylamino-benzaldehyde, Ber. Dtsch. Chem. Ges. A/B 60 (1927) 119–122.
[33] H.S. Gutowsky, C.H. Holm, Rate processes and nuclear magnetic resonance spectra. II. Hindered internal rotation of amides, J. Chem. Phys. 25 (1956) 1228–1234.
[34] M. Bollyn, Thermal hazards of the Vilsmeier–Haack reaction on N,N-dimethylaniline, Org. Process Res. Dev. 9 (6) (2005) 982–996.
[35] S.A.M.W. van den Broek, J.R. Leliveld, R. Becker, M.M.E. Delville, P.J. Nieuwland, K. Koch, F.P.J.T. Rutjes, Continuous flow production of thermally unstable intermediates in a microreactor with inline IR-analysis: controlled Vilsmeier–Haack formylation of electron-rich arenes, Org. Process Res. Dev. 16 (5) (2012) 934–938.
[36] C.A. Meriles, D. Sakellariou, H. Heise, A.J. Moulé, A. Pines, Approach to high-resolution ex situ NMR spectroscopy, Science 293 (2001) 82–85.
[37] H. Heise, D. Sakellariou, C.A. Meriles, A.J. Moulé, A. Pines, Two-dimensional high-resolution NMR spectra in matched B_0 and B_1 field gradients, J. Magn. Reson. 156 (1) (2002) 146–151.
[38] D. Topgaard, A. Pines, Self-diffusion measurements with chemical shift resolution in inhomogeneous magnetic fields, J. Magn. Reson. 168 (1) (2004) 31–35.
[39] D. Topgaard, D. Sakellariou, A. Pines, NMR spectroscopy in inhomogeneous B_0 and B_1 fields with non-linear correlation, J. Magn. Reson. 175 (1) (2005) 1–10.
[40] N. Sun, T.-J. Yoon, H. Lee, W. Andress, R. Weissleder, D. Ham, Palm NMR and 1-Chip NMR, IEEE J. Solid-State Circuits 46 (1) (2011) 342–352.
[41] D. Ha, J. Paulsen, N. Sun, Y.-Q. Song, D. Ham, Scalable NMR spectroscopy with semiconductor chips, PNAS 111 (33) (2014) 11955–11960.